The Effect of Rain on ERS Scatterometer Measurements

Congling Nie and David G. Long
Department of Electrical and Computer Engineering, Brigham Young University, Provo, Utah

***Abstract*— With the confirmed evidence of rain surface perturbation in recent studies of surface radar backscatter, the rain effects on C-band scatterometer measurements are reevaluated. By using co-located TRMM PR, WSAMI on ERS, and ECMWF data, we develop a low-order wind/rain backscatter model with inputs surface rain rate, incidence angle, and wind. We demonstrate that the wind/rain backscatter model is accurate enough for describing the total backscatter in raining areas with relatively low variance. We find that due to surface perturbation C-band ocean backscatter is more sensitive to rain than previously thought. Using three distinct regimes, we show under what conditions wind information, rain information, and both wind and rain can be retrieved from the measurements. We find that the effect of rain is more significant on the backscatter measurements at high incidence angles than at low incidence angles.**

I. Introduction

Rain is considered transparent to C-band scatterometer signals due to the fact that atmospheric attenuation and backscatter by rain for C-band scatterometer signals is negligibly small. However, recent studies reveal that surface effects of rain may significantly contribute to the total backscatter of C-band wind scatterometer measurements in rainy conditions [1] [2]. In a raining area, rain striking the water surface creates splash products from which the scatterometer signal scatters. The contribution of the splash products to the backscattering varies with incidence angle and polarization. At VV-polarization rain generated ring-waves are the dominant feature for radar backscattering at all incidence angles. On the other hand, raindrops impinging on the sea surface also generate turbulence in the upper water layer which attenuates the capillary wave spectrum. The modification of the ocean surface roughness by raindrops depends strongly on the wavelength of capillary waves. A study by Melsheimer et al. shows that the net effect of the impinging raindrops on the sea surface is a decrease of the amplitude of those water waves which have wavelengths above 10 cm and an increase of the amplitude of those water waves which have wavelengths below 5 cm [2]. The critical transition wavelength is not well defined, but it depends on the rain rate, the drop size distribution, the wind speed and the temporal evolution of the rain event [2]. Since the Bragg-wave scattering measured by scatterometer depends on incidence angle, the effect of rain on C-band scatterometer measurements varies with incidence angle and could be significant.

II. Wind/Rain Backscatter Model

To evaluate the effect of rain on data from the C-band wind scatterometer mode of the active microwave instrument (WSAMI) on ERS 1/2, a simple phenomenological wind/rain backscatter model [3] is used with co-located precipitation radar (PR) data from the Tropical Rainfall Measuring Mission (TRMM) satellite and numerical weather prediction (NWP) winds from European Center for Medium-Range Weather Forecasts (ECMWF). The model incorporates wind-induced surface scattering, surface rain perturbation, and atmospheric rain attenuation and scattering:

$$\sigma_m = (\sigma_{wind} + \sigma_{surf})\alpha_{atm} + \sigma_{atm} \tag{1}$$

where σ_m is the WSAMI measured σ°, σ_{wind} is the wind-induced surface backscatter, σ_{surf} is the rain-induced surface perturbation backscatter, α_{atm} is the two-way rain-induced atmospheric attenuation, and σ_{atm} is rain-induced atmospheric backscatter. The model is simplified by summing the attenuated surface perturbation and the atmospheric scattering terms, creating a single effective rain backscatter model,

$$\sigma_m = \sigma_{wind}\alpha_{atm} + \sigma_{eff} \tag{2}$$

where σ_{eff} is the total effective rain backscatter,

$$\sigma_{eff} = \sigma_{surf}\alpha_{atm} + \sigma_{atm}. \tag{3}$$

Co-located PR measurements enable computation of the WSAMI-observed surface rain rate, which is estimated by averaging the co-located PR surface rain rates over the WSAMI footprint, weighting each data point by the WSAMI response pattern. To estimate the two-way atmospheric rain attenuation on the WSAMI signal, we first estimate the atmospheric attenuation factor at the WSAMI wavelength (5.7 cm) by projecting the three dimensional rain rates of the TRMM 2A25 product through an empirical model. The path integrated attenuation (PIA) seen by the WSAMI at each TRMM PR measurement is computed by integrating the atmospheric attenuation factor through the PR antenna beam to the lowest no-surface-clutter range and adjusting the slant range to WSAMI slant range. Finally, the attenuation seen by WSAMI is calculated by averaging over the WSAMI footprint, weighting each data point by the WSAMI two-way antenna gain pattern.

In order to calculate an estimate of the atmospheric rain scattering, the effective reflectivity of the atmospheric rain is estimated from the TRMM 2A25 rain rate. Then, the volume backscattering coefficient without atmospheric attenuation is computed. The volume backscatter cross-section is adjusted by the WSAMI-seen two-way atmospheric attenuation factor. The total atmospheric rain backscatter observed by the WSAMI at each TRMM PR measurement is then calculated by integrating the volume backscatter cross-section through the PR antenna beam to the lowest no-surf-clutter range and adjusting to the WSAMI slant range. At last, the WSAMI-scale atmospheric rain scattering is computed by weighted-averaging all the atmospheric rain backscatter at each PR measurement over the WSAMI footprint.

An estimate of the wind-induced surface backscatter is computed via ECMWF predicted winds projected through WSAMI geophysical model function CMOD5. ECMWF predicted winds are interpolated in time and space to the center of each WSAMI measurement using cubic spline interpolation of the zonal and meridional components of the wind. The wind-induced surface backscatter derived from ECMWF has a bias introduced by prediction errors. We estimate the bias ϵ between ECMWF estimated σ° and WSAMI measured σ° for a specific antenna look direction, incidence angle, and ECMWF predicted wind speed bin using data from Jan 01, 2000 to Dec 31, 2000.

By combining the WSAMI, ECMWF NWP, and PR data, estimates of the surface rain perturbation and combined surface/atmospheric scattering are estimated by

$$\sigma_{surf} = \alpha_{atm}^{-1}(\sigma_m - \sigma_{atm}) - (\sigma_{wind(ECMWF)} + \epsilon). \quad (4)$$

Power-law (linear or quadratic log-log) models are used to relate the surface rain perturbation and combined surface/atmospheric scattering to WSAMI-observed surface rain rate $R_{surf(ant)}$. In order to estimate the parameters of the power-law models, nonparametric estimates of the surface rain perturbation and combined surface/atmospheric scattering are made as functions of rain rate at regular, logarithmically-spaced rain rate bins by using an Epanechnikov kernel [4]. The parameters are then computed by a linear or quadratic least-squares fit. For incidence angles less than 30°, the surface rain perturbation is not a monotonic function of surface rain rate and can not adequately be modeled by a simple linear or quadratic model. This suggests that the contributions of ring waves and turbulence are comparable under such conditions. For incidence angles greater than 30°, the contribution of ring waves dominates the surface effects of rain and the surface rain perturbation is monotonically increasing with surface rain rate. Since the Bragg wavelength of WSAMI at incidence angle higher than 30° are shorter than 5.8 cm, this result is close to the wavelength condition mentioned in [2]. For incidence angles between 30° to 40°, the variance of the estimate of σ_{surf} is relatively large, which makes the model unreliable. Thus, in this paper we only describe the model for incidence angles greater than 40°.

In the derivation of σ_{surf}, error is introduced by several sources. One of them is the prediction error of ECMWF predicted wind-induced backscatter $\sigma_{wind(ECMWF)}$. The procedure estimating α_{atm} and σ_{atm} from TRMM PR level 2A25 three dimensional rain rate introduces additional errors due to the error of the empirical model functions, nonuniform beam filling (NUBF), and temporal and spatial mismatch between WSAMI and TRMM PR measurements. We adopt the combined rain model of equation 2 to reduce the influence of the error. It is also noted that our interest is in the total effect of rain in wind retrieval. The corresponding power law model of σ_{eff} is

$$10log_{10}(\sigma_{eff}) \approx f_e(R_{dB}) = \sum_{n=0}^{N} x_e(n) R_{dB}^n. \quad (5)$$

where $R_{dB} = 10log_{10}(R_{surf(ant)})$, $x_e(n)$ are model coefficients. $N = 1$ for the linear model, and $N = 2$ for the quadratic model. The values of $x_e(n)$ are calculated using the same method mentioned before. Figure 1 shows the nonparametric fits of σ_{eff} and linear/quadratic fits of the nonparametric fits in log-log space for different incidence angle bins.

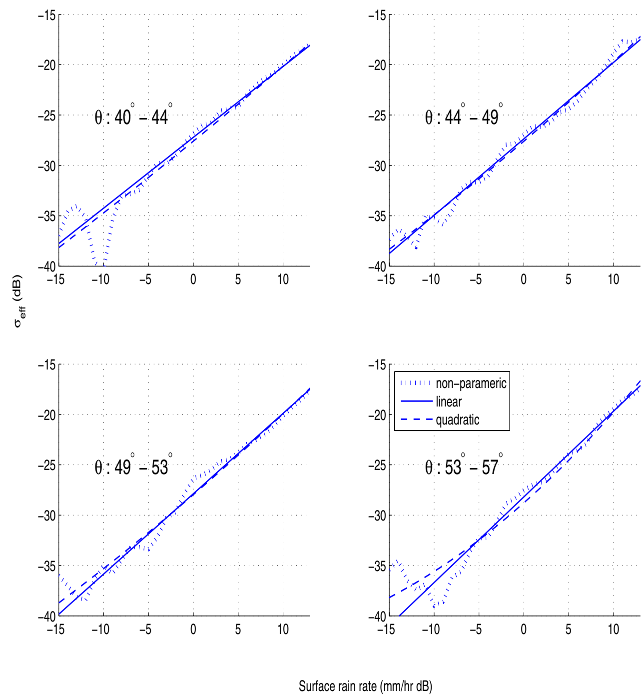

Fig. 1. Linear and quadratic fits to the non-parametric fits of effective rain backscatter σ_{eff} in log-log space for different incidence angle bins. Non-parametric fits are also plotted.

III. Model Validation

To validate the model, we do a non-parametric estimate of both WSAMI measured backscatter $\sigma_{m(WSAMI)}$ and model estimated backscatter $\sigma_{m(model)}$ on a regular grid with axes of $\sigma_{wind(ECMWF)} + \epsilon$ and R_{dB} using a two-dimensional Epanechnikov kernel with a bandwidth of 3 dB for different incidence angle bins. $\sigma_{m(model)}$ is calculated using the quadratic combined rain model. A log error is computed by $\sigma_{m(model)} - \sigma_{m(WSAMI)}$. Figure 2 shows the nonparametric estimates of $\sigma_{m(WSAMI)}$, $\sigma_{m(model)}$ with respect to $\sigma_{wind(ECMWF)} + \epsilon$ and R_{dB} for different incidence angle bins. For the two incidence angle bins, the model estimated backscatter is very close to the WSAMI measured backscatter, with a log error within ± 2 dB. It is noted that the largest error occurs at high rain rates due to less data at high rain rates, which increases the uncertainty in the estimate. For θ ranging from $40°$ to $49°$, 95% of the model predicted backscatter is within 3dB of the WSAMI measured backscatter, while the standard deviation of the log error is about 1.4 dB. For θ ranging from $49°$ to $57°$, the percentage is 91% and the standard deviation is about 1.6 dB. The relatively low variances show that the model is sufficient for describing the total backscatter in raining areas.

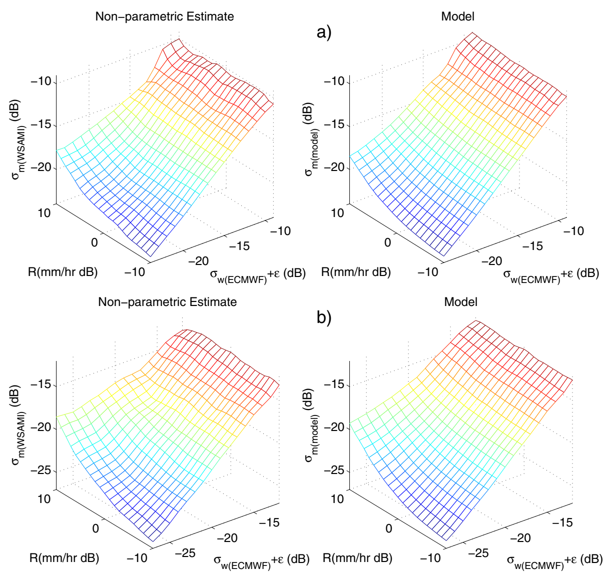

Fig. 2. Nonparametric and combined rain effect models for a) $40° - 49°$ and b) $49° - 57°$. The error between parametric and nonparametric models are also shown.

To understand the effect of rain on the scatterometer measurements for different incidence angles, following [3] we define three distinct backscatter regimes. In regime 1, rain-induced backscatter dominates the total backscatter. Regime 2 is where the rain-induced backscatter and wind-induced backscatter are on the same order of magnitude. In regime 3, wind-induced backscatter dominates the total backscatter. It is noted that it may be possible to simultaneously estimate wind and rain information from regime 2, while in regime 1 or regime 2, only the dominating parameter (wind or rain) can be retrieved. We identify these regimes by thresholding the ratio $\tau = \sigma_{eff}/\sigma_m$. Approximately, we define regime 1 by $\tau > 0.75$, regime 3 as $\tau < 0.25$, and regime 2 as $0.25 \leq \tau \leq 0.75$. In Figure 3, we plot the τ computed using combined wind/rain model with respect to surface rain rate R_{dB} and wind-only backscatter σ_{wind}, with three regimes shown in different colors. We also plot contours of the predicted total backscatter σ_m in solid line and contours of σ_{wind} in dashed lines on the same figure. It is noted that with the increasing of R_{dB}, the curve of σ_m deviate from the curve of σ_{wind}. As incidence angle increases, the area of regime 1 reduces while the area of regime 3 increases, suggesting that rain has more significant impact on the WSAMI measurements at higher incidence angle.

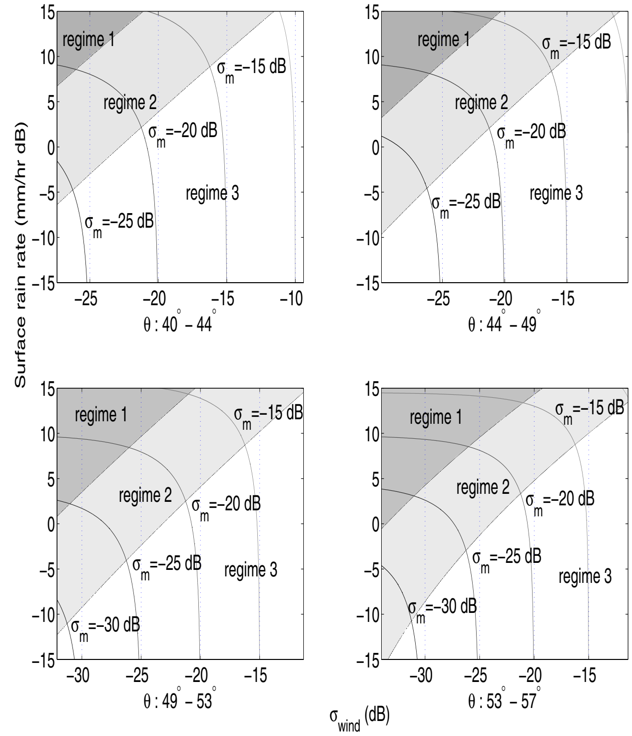

Fig. 3. Backscatter regimes for WSAMI as a function of rain rate and effective wind backscatter for several incidence angles. Also plotted is a contour plot of the combined rain effect model for σ_m.

IV. Conclusions

With confirmed evidence of rain surface perturbation, the rain effects on C-band scatterometer measurements are reevaluated. By using co-located TRMM PR, WSAMI on ERS, and ECMWF data, the parameters of a low-order wind/rain backscatter model are estimated for the surface rain rate, incidence angle, and wind. The wind/rain backscatter model is accurate enough for describing the total backscatter in raining areas with relatively low variance. We find that due to surface perturbation effects, at high incidence angle C-band $\sigma°$ is more sensitive to rain than generally believed. In low wind speed and heavy rain conditions, rain has significant impact on $\sigma°$ at high incidence angle.

References

[1] Nicole Braun, Martin Gade, Philipp A. Lange, Radar backscattering measurements of artificial rain impinging on a water surface at different wind speeds, *Proceedings of the 1999 International Geoscience and Remote Sensing Symposium (Hamburg, Germany)*, 1963-1965, IEEE Press. Piscataway, N.J., 1999

[2] Christian Melsheimer, Werner Alpers, Martin Gade, Simultaneous observations of rain cells over the ocean by the synthetic aperture radar aboard the ERS satellites and by surface-based weather radars, *Journal of Geophysical Research*, Vol. 106 No. C3, 4665-4677, 2001

[3] David W. Draper, David G. Long, Evaluating the effect of rain on SeaWinds scatterometer measurements, *Journal of Geophysical Research*, Vol. 109, C02005, 2004.

[4] M. P. Wand, and M. C. Jones, *Kernel Smoothing*, Chapman & Hall, 1995.